AIAA JOURNAL
Vol. 34, No. 4, April 1996

Aeroelastic Optimization of a Helicopter Rotor with Two-Cell Composite Blades

Ranjan Ganguli* and Inderjit Chopra†
University of Maryland, College Park, Maryland 20742

Aeroelastic and sensitivity analyses of the rotor based on a finite element in space and time are linked to an automated optimization algorithm to perform optimization studies for a four-bladed, soft in-plane composite rotor consisting of a two-cell thin-walled beam. The design variables used in this study are the ply angles of the laminated walls of the composite beam. The objective function minimizes the 4/rev hub loads, with constraints on blade frequencies and aeroelastic stability in forward flight. Optimum design solutions show a reduction in the objective function of about 20% due to elastic stiffnesses and an additional 13% due to composite couplings. Starting from an initially infeasible design, the optimum design solution with negative lag bending-torsion coupling results in an increase in lag mode damping of about 140% compared to the baseline layup.

Nomenclature

C_d, C_l, C_m	= drag, lift and pitching moment coefficient
C_T	= thrust coefficient
c	= blade chord
D_j	= blade section properties
EA	= blade axial stiffness
EI_y	= blade flap bending stiffness
EI_z	= blade lag bending stiffness
F_{xH}^{4P}, F_{yH}^{4P}, F_{zH}^{4P}	= 4/rev longitudinal, lateral, and vertical force
GJ	= blade torsional stiffness
$\boldsymbol{g}$	= constraints
J	= objective function
$\boldsymbol{K}^s$	= structural stiffness matrix
$\bar{k}$	= blade composite couplings
$\bar{k}_{23}$	= blade flap bending-torsion composite couplings
$\bar{k}_{24}$	= blade lag bending-torsion composite couplings
M_{xH}^{4P}, M_{yH}^{4P}, M_{zH}^{4P}	= 4/rev rolling, pitching, and yawing moment
$\boldsymbol{M}^s$	= structural mass matrix
m_0	= reference mass per unit length
N	= number of beam finite elements
R	= rotor radius
T	= kinetic energy
U	= strain energy
u_e	= axial deformation of blade
v_b	= lag deformation of blade
W	= virtual work
w_b	= flap deformation of blade
$\boldsymbol{x}$	= normalized complex eigenvector of transition matrix
Y	= blade response
α	= angle of attack at blade section
α_k	= real part of characteristic exponent of kth mode
β	= flap angle
ϵ_k	= minimum acceptable level of damping for kth mode
ϵ_{xz}, ϵ_{yz}	= transverse shear strains
ζ	= web location of the two-cell box-beam, lag angle
θ	= ply angle design variables
λ_k	= eigenvalue of kth stability mode
μ	= advance ratio
σ	= solidity ratio
Φ	= mode shape
ϕ	= torsional deformation of blade
Ψ	= Floquet state transition matrix
ψ	= azimuth angle, time
Ω	= rotation speed
ω	= blade rotating frequencies

Subscripts

F	= flap mode
L	= lag mode
T	= torsion mode

Superscripts

L	= lower bound
R	= real part
U	= upper bound

Received Dec. 1, 1994; revision received April 25, 1995; accepted for publication April 25, 1995.

*Assistant Research Scientist, Center for Rotorcraft Education and Research, Department of Aerospace Engineering. Member AIAA.

†Professor and Director, Center for Rotorcraft Education and Research, Department of Aerospace Engineering. Fellow AIAA.

Introduction

HELICOPTER rotor blades are now routinely built using composite materials because of their superior fatigue characteristics and stiffness/weight ratio compared to metals. However, the helicopter industry designs the composite blades as isotropic beams and has not yet exploited the tailorability of composite couplings. Research over the past few years has shown that composite rotor designs with elastic coupling can significantly influence vibrations and enhance aeromechanical stability of the rotor-fuselage system.[1–4] The objective of this paper is to apply an optimization methodology to reduce vibration of helicopters by tailoring elastic couplings and stiffnesses of composite rotor blades having generic, multicell cross sections.

Over the past few years, considerable research has been directed toward the application of aeroelastic optimization methodology to design rotors with low vibration.[5] The research conducted ranges from simple analysis neglecting aeroelastic couplings to comprehensive studies using refined aeroelastic and sensitivity analysis. The complexity and computational expense associated with an aeroelastic optimization has led some researchers to formulate simpler strategies for vibration reduction in helicopters, such as blade rotating frequency placement and modal-based vibration methods. However, it has been shown that frequency placement is not a reliable means for obtaining vibration reduction.[6] On the other hand, minimization of modal vibration indices and modal hub shears lead

to a reduction in the vibratory hub loads; this result has also been verified by wind-tunnel tests comparing a baseline rotor to the optimum rotor.[6]

Modal based optimization methods such as those used in the cited studies are computationally inexpensive and easy to implement. However, such methods often neglect the aeroelastic interactions (between the airloads and the blade response). Therefore, the optimization procedure minimizes the vibratory hub loads by tailoring the blade response to an assumed airload distribution. The assumptions involved in modal-based optimization can be avoided by using an aeroelastic optimization procedure based on a comprehensive aeroelastic analysis. Typically, the use of such optimization algorithms requires calculation of the gradient of the objective function and constraints. These gradients are needed by optimization algorithms to determine the search direction along which the objective function decreases without violating the constraints. Most of the studies on aeroelastic optimization of helicopter rotors, use finite difference methods for calculating these gradients. Because of large computer time requirements, such studies are restrictive in terms of the objective function, constraints, and design variables.

This aspect has challenged researchers to develop alternative approaches for calculating the sensitivity derivatives. Celi and Friedmann[7] used approximation techniques[8] to perform aeroelastic optimization. They minimized the oscillatory vertical hub shear for a hingeless rotor with both straight and swept tips while imposing constraints on frequency placements and blade stability in hover. Design variables used in this study include thickness and chordwise length of cross sections, offsets of the aerodynamic center, and center of gravity from the elastic axis and tip sweep. Results show that approximation methods are an efficient approach to optimization when compared to finite differencing.

An analytical scheme for calculating the sensitivity derivatives of the objective function and constraints was formulated by Lim and Chopra[9] to minimize all six vibratory hub shears and moments with constraints on blade stability in forward flight. Design variables include placement of nonstructural mass along the blade span, the offset of nonstructural mass from the elastic axis, and the spanwise distribution of flap, lag, and torsion stiffnesses. This approach also resulted in considerable savings of computation time compared to the finite difference approach.

Conducting aeroelastic optimization of a composite rotor requires accurate analytical tools to model its structural behavior. Typically, an aeroelastic analysis of a composite rotor can be broken into two parts: calculation of blade section structural properties and calculation of coupled rotor aeroelastic analysis. The first part of calculation of section properties is carried out in a stand-alone uncoupled blade analysis, and then in the second part, these section properties are used as inputs to perform a coupled rotor aeroelastic analysis.

Research on the structural modeling of composite rotor blades has evolved along two directions: the detailed finite element models[10] and the analytical models.[11] Whereas finite element methods are more versatile and flexible than analytical methods, they are computationally more involved. Direct analytical models are simple and efficient, and appear attractive to implement in a comprehensive rotor aeroelastic analysis, especially to carry out optimization studies.

So far, only a few researchers have carried out the aeroelastic analysis of composite rotors. Early work[1,2] on the aeroelastic behavior of coupled composite blades showed that the structural coupling due to ply layup can have a powerful influence on aeroelastic stability, blade stresses, and loads. These works, however, did not precisely model the nonclassical effects such as transverse shear that can become important for composite blades.[12] Smith and Chopra[3,4] addressed this limitation by extending the earlier analyses to include effects of transverse shear using additional degrees of freedom (DOF) in the blade equations, resulting in an extended finite element representation (19 DOF instead of 15 DOF). The size and complexity of the aeroelastic code, however, was increased considerably because of additional DOF. Using static condensation of shear degrees of motion, Nixon and Hinnant[14] showed that essential structural stiffness and coupling can be captured. This approximation helps to reduce the finite element DOF from 19 to 15 and, hence, will be exploited in this investigation.

Many composite beam models have been developed for thin-walled, single-cell box beams. Production rotor blades, however, are built as multicell airfoil sections. Since single-cell representation of a multicell rotor blade can result in an overestimation of the torsional flexibility,[13] it is important to model it as a multicell beam. Chandra and Chopra[12] have developed an analysis based on Vlasov theory for thin-walled composite beams of arbitrary sections including open sections, closed single-cell sections and multicell sections. The model includes the effect of out-of-plane warping deformation of the cross section, transverse-shear related couplings, and constraining the warping deformation at the edges. The results of this analysis were validated by Chandra and Chopra[12] with experiments for the structural response and free vibration characteristics of coupled composite beams including I-beams, box-beams, and two-cell blades.

The objectives of this paper are 1) to implement a refined composite blade analysis into a comprehensive rotor aeroelastic analysis, 2) to develop a semianalytical sensitivity analysis and optimization capability for composite rotor blades with generic sections, and 3) to couple the sensitivity analysis with optimization algorithms to conduct an aeroelastic optimization to minimize vibratory hub loads and enhance blade stability.

For the numerical study, a soft in-plane, four-bladed hingeless rotor is used. The blade is modeled as a two-cell box-beam spar. Design variables are the ply angles of the laminated walls of the spar. Sensitivity derivatives of blade response, rotating frequencies, hub loads, and blade stability are calculated analytically as an integral part of the aeroelastic response and stability analysis. The aeroelastic optimization problem consists of minimization of a weighted sum of 4/rev oscillatory hub loads subject to constraints on blade rotating frequencies and aeroelastic stability in forward flight.

Composite Rotor Aeroelastic Analysis

A composite beam analysis developed by Chandra and Chopra[12] and capable of modeling blades with generic cross sections is used for this study.

Composite Beam Analysis

Static condensation is used to eliminate shear related DOF. Then, relations between the generalized forces and displacements can be written as

$$\begin{bmatrix} Q_x \\ M_x \\ -M_y \\ M_z \end{bmatrix} = \begin{bmatrix} EA & \bar{k}_{12} & \bar{k}_{13} & \bar{k}_{14} \\ \bar{k}_{12} & GJ & \bar{k}_{23} & \bar{k}_{24} \\ \bar{k}_{13} & \bar{k}_{23} & EI_y & \bar{k}_{34} \\ \bar{k}_{14} & \bar{k}_{24} & \bar{k}_{34} & EI_z \end{bmatrix} \begin{bmatrix} u_e' \\ \phi' \\ w_b'' \\ v_b'' \end{bmatrix} \tag{1}$$

For an isotropic blade, the off-diagonal terms in the stiffness matrix are zero. Coupled composite blades have nonzero off-diagonal terms.

Aeroelastic Analysis

The finite element analysis for the rotor blade is based on Hamilton's principle. After discretization using 15 DOF beam elements, the Hamilton's principle can be written as

$$\delta\Pi = \int_{\psi_1}^{\psi_2} (\delta U - \delta T - \delta W)\, d\psi$$

$$= \int_{\psi_i}^{\psi_f} \sum_{i=1}^{N} (\delta U_i - \delta T_i - \delta W_i)\, d\psi = 0 \tag{2}$$

Blade energy expressions are derived for a generic composite beam, such as defined by Eq. (1). Expressions for the virtual strain energy are derived for a beam undergoing moderate deflections. Expressions for the virtual kinetic energy and virtual work are the same as isotropic blades. The effect of composite materials comes in only through the strain energy variational.

The aeroelastic analysis involves the calculation of the vehicle trim, steady response, and stability of the rotor-body perturbation motion. The steady periodic blade response is calculated using a

finite element method in time after the nonlinear equations in space are transformed into normal mode equations. The nonlinear vehicle trim and blade response equations are solved iteratively as a coupled solution. The linearized periodic rotor perturbation equations are solved using Floquet transition matrix theory. For details on the aeroelastic analysis, see Ref. 16.

Optimization Analysis

A general mathematical optimization problem is of the following form: Minimize the objective function $J(\theta)$ subject to the constraints $\boldsymbol{g}(\theta) \leq \mathbf{0}$ and move limits $\theta^L \leq \theta \leq \theta^U$.

Objective Function

For a helicopter rotor with N_b blades, an important source of vibration is the N_b/rev hub forces and moments transmitted by the rotor to the fuselage. For a four-bladed rotor, the objective function is chosen as a combination of the magnitudes of the 4/rev harmonics of the three forces (longitudinal, lateral, and vertical) and three moments (pitch, roll, and yaw):

$$J = \sqrt{\left(F_{xH}^{4P}\right)^2 + \left(F_{yH}^{4P}\right)^2 + \left(F_{zH}^{4P}\right)^2} + \sqrt{\left(M_{xH}^{4P}\right)^2 + \left(M_{yH}^{4P}\right)^2 + \left(M_{zH}^{4P}\right)^2} \tag{3}$$

The forces and moments are nondimensionalized by dividing with $m_0\Omega^2R^2$ and $m_0\Omega^2R^3$, respectively.

Design Variables

Ply angles of the laminated walls of the box beam are used as design variables. They are denoted by θ_i, $i = 1, n$. It is assumed that all of the walls have the same number of plies. Depending on the nature of the layup (balanced, symmetric, and antisymmetric), the ply angles of various walls may be related.

Behavior Constraints

The behavior constraints considered in this study are 1) aeroelastic stability and 2) frequency placement. The aeroelastic stability constraint keeps the rotor blade stable at a particular flight condition, and for the kth mode, can be expressed as $g_s(\theta) = \alpha_k + \epsilon_k \leq 0$, where

$$\alpha_k = \ell_n \sqrt{\left(\lambda_k^R\right)^2 + \left(\lambda_k^I\right)^2}/2\pi$$

The λ_k^R and λ_k^I are calculated by solving the following complex eigenvalue problem: $\lambda x = \Psi(\psi_0+2\pi, \psi_0)x$, where $\Psi(\psi_0+2\pi, \psi_0)$ is the transition matrix at the end of one time period ($T = 2\pi$) and ψ_0 is the initial time.

The frequency placement constraint keeps the first flap, lag, and torsion frequencies within realistic boundaries. The frequency constraint for the kth mode can be expressed as $g_f^L(\theta) = 1-\omega_k/\omega_k^L \leq 0$ and $g_f^U(\theta) = 1-\omega_k/\omega_k^U \geq 0$, where ω_k is obtained from the solution of the eigenvalue problem: $\boldsymbol{K}^s\Phi = \omega_k^2\, M^s\Phi$.

Sensitivity Analysis

The sensitivity derivatives of the objective function and behavior constraints are required by the optimization algorithms. Consider a general function F, which could be the objective function J, the frequency constraints $\boldsymbol{g}_f$, or the stability constraints $\boldsymbol{g}_s$. Since F is a function of both the blade section properties D_j and the blade response Y, differentiating F with respect to the design variable θ_i and applying chain rule differentiation yields

$$\frac{\mathrm{d}F}{\mathrm{d}\theta_i} = \frac{\mathrm{d}F}{\mathrm{d}D_j}\frac{\partial D_j}{\partial \theta_i} = \left(\frac{\partial F}{\partial D_j} + \frac{\partial F}{\partial Y}\frac{\partial Y}{\partial D_j}\right)\frac{\partial D_j}{\partial \theta_i} \tag{4}$$

where $D_j = \lfloor EA, \bar{k}_{12}, \bar{k}_{13}, \bar{k}_{14}, GJ, \bar{k}_{23}, \bar{k}_{24}, EI_y, \bar{k}_{34}, EI_z \rfloor$ are all of the stiffness and coupling constants contained in the virtual strain energy. Since the computational effort involved with the calculation of section properties of a composite blade is very small, it is convenient to use finite difference approximations to calculate the derivatives $\partial D_j/\partial\theta_i$. The derivatives $\mathrm{d}F/\mathrm{d}D_j$ are calculated as an integral part of the aeroelastic analysis using a direct analytical approach.[17] Then using Eq. (4), the sensitivity derivative of F with respect to θ_i can be calculated. This approach may be called semianalytical because both finite difference and analytical derivatives are used to calculate the gradients.

Results and Discussion

For the numerical study, a four-bladed, soft in-plane uniform hingeless composite rotor is considered. The rotor properties are given in Table 1. For the analysis, the blade is divided into five equally spaced finite elements. For discretization in the time domain, four temporal finite elements with quartic polynomial distribution within each element are used. A stability analysis is performed in the rotating frame using the Floquet transition matrix theory, and the fourth-order Runge–Kutta method is used for calculating the transition matrix and its derivatives. Eight normal modes (three flap, two lag, two torsion, and one axial) are used for the trim analysis, and seven modes (three flap, two lag, and two torsion) are used for the stability analysis. Results are obtained at a forward speed of $\mu = 0.3$ and a C_T/σ of 0.07.

The blade spar is made of graphite/epoxy (AS4/3501-6) plies, the properties of which are shown in Table 2. Optimization results are obtained for a two-cell composite box beam, the dimensions of which are shown in Fig. 1. By choosing different ply layups shown in Table 3, selected couplings can be introduced. These layups are five two-cell thin-walled beam configurations with five walls each: top, bottom, left, right, and the web. The configuration consisting of balanced laminates with no elastic couplings is designated as uncoupled A (Table 3). Ply orientation angles used in defining the layups are positive toward the leading edge for the horizontal spar walls (top and bottom) and positive toward the bottom for the vertical spar walls. The uncoupled A configuration is used as a starting point in this study. Flapwise bending-torsion coupling (pitch-flap coupling) can be introduced in this layup by unbalancing the top and bottom walls of the beam. Chordwise bending-torsion coupling (pitch-lag coupling) can be introduced by unbalancing the side walls of the beam. The symmetric A and symmetric B layups (Table 3) exhibit positive and negative pitch-flap couplings, respectively. The symmetric C and symmetric D (Table 3) layups display positive

Table 1 Rotor properties

Number of blades	4
Radius, ft	16.2
Hover tip speed, ft/s	650
C_l	$5.73\,\alpha$
C_d	$0.0095 + 0.2\,\alpha^2$
C_m	0.0
c/R	0.08
Solidity, σ	0.10
C_T/σ	0.07
Precone β_p	0.0
Lock number, γ	6.34
Blade pretwist	0.0

Table 2 Composite spar properties

Longitudinal modulus E_L, msi	20.59
Transverse modulus E_T, msi	1.42
Shear modulus G_{LT}, msi	0.87
Major Poisson ratio ν_{LT}	0.42

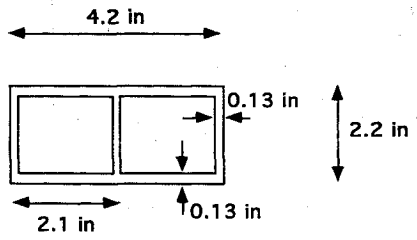

Fig. 1 Cross-sectional dimensions for the box beam.

Table 3 Layups for optimization study

	Uncoupled A, no coupling
Top	$[0_3/(\theta_1/-\theta_1)/(\theta_2/-\theta_2)/(\theta_3/-\theta_3)/(45/-45)_2]_s$
Bottom	$[0_3/(\theta_1/-\theta_1)/(\theta_2/-\theta_2)/(\theta_3/-\theta_3)/(45/-45)_2]_s$
Left	$[0_3/(\theta_1/-\theta_1)/(\theta_2/-\theta_2)/(\theta_3/-\theta_3)/(45/-45)_2]_s$
Right	$[0_3/(\theta_1/-\theta_1)/(\theta_2/-\theta_2)/(\theta_3/-\theta_3)/(45/-45)_2]_s$
Web	$[0_3/(\theta_1/-\theta_1)/(\theta_2/-\theta_2)/(\theta_3/-\theta_3)/(45/-45)_2]_s$
	Symmetric A, positive flap bending-torsion coupling
Top	$[0_3/(\theta_1/\theta_1)/(\theta_2/\theta_2)/(\theta_3/\theta_3)/(45/-45)_2]_s$
Bottom	$[0_3/(\theta_1/\theta_1)/(\theta_2/\theta_2)/(\theta_3/\theta_3)/(45/-45)_2]_s$
Left	$[0_3/(\theta_1/-\theta_1)/(\theta_2/-\theta_2)/(\theta_3/-\theta_3)/(45/-45)_2]_s$
Right	$[0_3/(\theta_1/-\theta_1)/(\theta_2/-\theta_2)/(\theta_3/-\theta_3)/(45/-45)_2]_s$
Web	$[0_3/(\theta_1/-\theta_1)/(\theta_2/-\theta_2)/(\theta_3/-\theta_3)/(45/-45)_2]_s$
	Symmetric B, negative flap bending-torsion coupling
Top	$[0_3/(-\theta_1/-\theta_1)/(-\theta_2/-\theta_2)/(-\theta_3/-\theta_3)/(45/-45)_2]_s$
Bottom	$[0_3/(-\theta_1/-\theta_1)/(-\theta_2/-\theta_2)/(-\theta_3/-\theta_3)/(45/-45)_2]_s$
Left	$[0_3/(\theta_1/-\theta_1)/(\theta_2/-\theta_2)/(\theta_3/-\theta_3)/(45/-45)_2]_s$
Right	$[0_3/(\theta_1/-\theta_1)/(\theta_2/-\theta_2)/(\theta_3/-\theta_3)/(45/-45)_2]_s$
Web	$[0_3/(\theta_1/-\theta_1)/(\theta_2/-\theta_2)/(\theta_3/-\theta_3)/(45/-45)_2]_s$
	Symmetric D, negative lag bending-torsion coupling
Top	$[0_3/(\theta_1/-\theta_1)/(\theta_2/-\theta_2)/(\theta_3/-\theta_3)/(45/-45)_2]_s$
Bottom	$[0_3/(\theta_1/-\theta_1)/(\theta_2/-\theta_2)/(\theta_3/-\theta_3)/(45/-45)_2]_s$
Left	$[0_3/(\theta_1/\theta_1)/(\theta_2/\theta_2)/(\theta_3/\theta_3)/(45/-45)_2]_s$
Right	$[0_3/(\theta_1/\theta_1)/(\theta_2/\theta_2)/(\theta_3/\theta_3)/(45/-45)_2]_s$
Web	$[0_3/(\theta_1/-\theta_1)/(\theta_2/-\theta_2)/(\theta_3/-\theta_3)/(45/-45)_2]_s$
	Symmetric C, positive lag bending-torsion coupling
Top	$[0_3/(\theta_1/-\theta_1)/(\theta_2/-\theta_2)/(\theta_3/-\theta_3)/(45/-45)_2]_s$
Bottom	$[0_3/(\theta_1/-\theta_1)/(\theta_2/-\theta_2)/(\theta_3/-\theta_3)/(45/-45)_2]_s$
Left	$[0_3/(-\theta_1/-\theta_1)/(-\theta_2/-\theta_2)/(-\theta_3/-\theta_3)/(45/-45)_2]_s$
Right	$[0_3/(-\theta_1/-\theta_1)/(-\theta_2/-\theta_2)/(-\theta_3/-\theta_3)/(45/-45)_2]_s$
Web	$[0_3/(\theta_1/-\theta_1)/(\theta_2/-\theta_2)/(\theta_3/-\theta_3)/(45/-45)_2]_s$

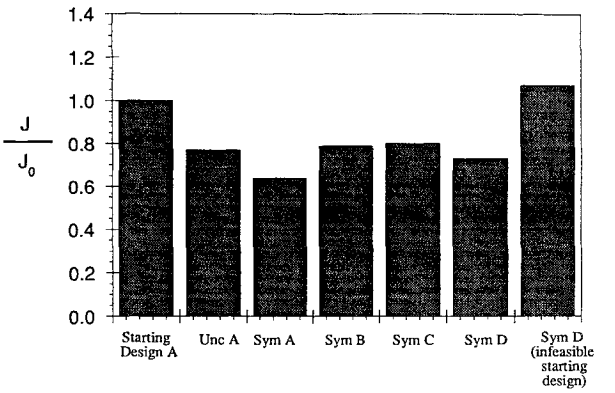

Fig. 2 Objective function corresponding to initial and optimum designs, normalized with starting design A values.

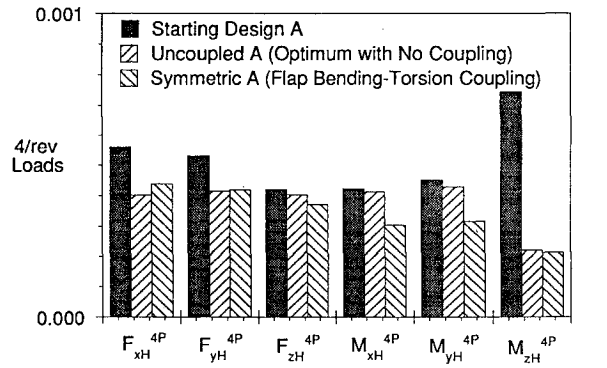

Fig. 3 Vibratory hub loads corresponding to initial and optimum designs.

and negative pitch-lag couplings, respectively. The magnitude of the coupling depends on the values of the angles θ_1, θ_2, and θ_3.

The design variables are the ply angles θ_1, θ_2, and θ_3. The 0- and 45-deg plies are unchanged to assure that the optimum design does not become unrealistic. Move limits are placed on the design variables: $\theta^L = \theta_{i-1} - 15(0.9)^{i-1}$ and $\theta^U = \theta_{i-1} + 15(0.9)^{i-1}$, where i is the iteration number. The values 15 and 0.9 in the preceding equation were suggested by Watkins and Morris[17] for good numerical stability and convergence.

Typically, ply angles influence both elastic stiffnesses and elastic couplings. To filter the effect of elastic coupling on the optimum design, optimization is performed for both uncoupled and coupled layups: The uncoupled optimum reflects the influence of elastic stiffness only and is used as a baseline design with which the coupled optimum designs are compared.

The optimization is performed to minimize the objective function J defined by Eq. (3). The upper and lower bounds on the first lag, flap and torsion frequencies are $0.60/\text{rev} \le \omega_{1L} \le 0.80/\text{rev}$, $1.08/\text{rev} \le \omega_{1F} \le 1.18/\text{rev}$, and $2.50/\text{rev} \le \omega_{1T} \le 6.50/\text{rev}$. For the stability constraint, ϵ_k is chosen to be zero. The stability constraint is applied on the first flap, lag, and torsion modes. The optimization study is conducted using the optimizer CONMIN.[15]

Optimization of Uncoupled Layup

The optimization for the uncoupled A layup is started from $\theta_1 = 15$, $\theta_2 = 30$, and $\theta_3 = 15$ deg. This design (called starting design A) is feasible and the optimizer shows good convergence characteristics when starting from this design. The objective function J is reduced by over 20% relative to starting design A (see Fig. 2) and the resulting layup is called the uncoupled A optimum design. The 4/rev hub loads corresponding to starting design A, the uncoupled A optimum design and the symmetric A optimum design are shown in Fig. 3. The results for the symmetric A layup are discussed later. From Fig. 3, it can be seen that compared to starting design A, there is a reduction in all of the six 4/rev hub forces and moments for the uncoupled A optimum design and, in fact, a reduction of over 70% in the 4/rev yawing moment. Since the uncoupled A layup displays no elastic coupling, these reductions in the vibratory hub loads are due to changes in elastic stiffness only. The optimum design variables obtained after roundoff to the nearest integer are $\theta_1 = 4$, $\theta_2 = 14$, and $\theta_3 = 5$ deg. The uncoupled A optimum design is used as a benchmark with which the coupled optimum designs are compared.

Throughout this optimization study, ply angles obtained from the optimization process are rounded off to the nearest integer values. The aeroelastic analysis is then performed with these integer ply angles. Laminates with such ply angles can be fabricated using automated composite manufacturing techniques.

During composite manufacturing, small errors may be incurred in the ply layup. For the optimum design to be practical, small variations of the ply angles from the optimum design should not cause a large change in the objective function. It is found that roundoff of the ply angles causes very small change in the objective function. To further investigate the robustness of the optimum design, the design variables for the uncoupled A design (obtained earlier) are increased by 1 deg each; this causes a change in J of only 0.07% from the optimum value. Again, this shows that the optimum design is robust and manufacturing of such layups is feasible.

Optimization of Coupled Layups

The optimum design angles from the uncoupled A layup are used as the initial guess for performing optimizations on the symmetric A, symmetric B, symmetric C, and symmetric D layups. The symmetric A layups shows a further reduction of 13% in the objective function J from the uncoupled A optimum design, and the symmetric C layup shows a reduction of 4% (Fig. 2). Compared to the uncoupled A optimum, the symmetric B, and symmetric D layups show no reduction in the objective function. Detailed results for symmetric C, symmetric B, and symmetric D are not shown because of the small/negligible reduction in the objective function for these cases.

Comparing the 4/rev hub forces and moments for the uncoupled A optimum design and the symmetric A optimum designs (Fig. 3) shows a reduction in the 4/rev vertical hub shear and the 4/rev rolling, pitching, and yawing moments; however, there is a small increase

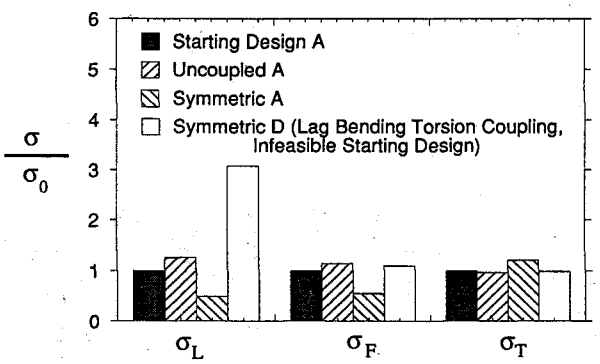

Fig. 4 Damping of first lag, flap, and torsion modes corresponding to initial and optimum designs, normalized by starting design A values.

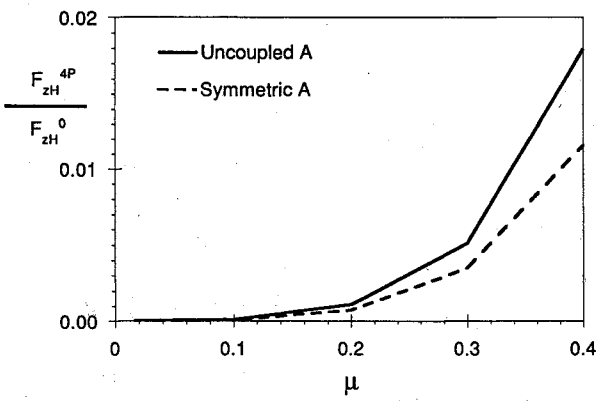

Fig. 5 Comparison of vibratory vertical hub shear between the uncoupled A and symmetric A optimum designs, normalized with steady thrust; design condition is $\mu = 0.3$.

in the 4/rev longitudinal and lateral forces. The optimum design variables for the symmetric A optimum design are $\theta_1 = 9$, $\theta_2 = 22$, and $\theta_3 = 10$ deg.

The benefits of using elastic stiffness and composite coupling for reduction in vibratory hub loads is clear from Fig. 3. Comparing the starting design A to the symmetric A design, the 4/rev longitudinal, lateral, and vertical forces are reduced by 21, 22, and 12%, respectively, and the 4/rev rolling, pitching and yawing moments are decreased by 29, 31 and 71%, respectively.

Figure 4 shows the damping of the first lag, flap, and torsion modes for several different layups. The symmetric D layup with infeasible starting design is discussed later. Compared to the starting design A, the uncoupled A optimum design shows a small increase in the lag and flap damping and a very small reduction in the torsion damping. For the symmetric A optimum design, there is a decrease in the lag and flap mode damping and an increase in the torsion mode damping, compared to both the starting design A and the uncoupled A optimum. Note that the dampings shown in Fig. 4 are normalized with starting design A values: $\sigma_L = 0.0099$, $\sigma_F = 0.488$, and $\sigma_T = 0.932$. It is clear that the flap and torsion modes are highly damped and the lag mode is low damped.

The preceding optimization solutions are calculated for an advance ratio of 0.3. It is interesting to investigate if these optimum designs also yield reductions in the vibratory hub loads at off-design conditions. As an example, the 4/rev vertical hub shear and the 4/rev hub rolling moment are shown for the uncoupled A and symmetric A optimum designs at different advance ratios in Figs. 5 and 6, respectively. There is a reduction in the vibratory hub loads throughout the forward speed range. In fact, at $\mu = 0.4$, the reduction is significantly more than at $\mu = 0.3$, showing that positive flap bending-torsion coupling is increasingly beneficial for vibration reduction as forward speed increases.

To understand the rationale behind the reduction in vibratory hub loads due to composite coupling, the flap, lag, and torsion responses at the blade tip are compared for the uncoupled A optimum design and the symmetric A optimum design as shown in Fig. 7. There is a

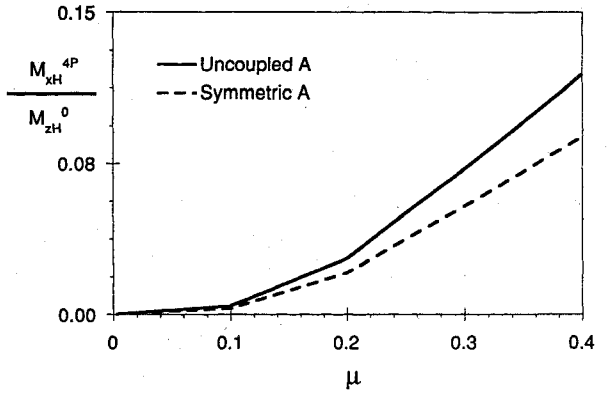

Fig. 6 Comparison of vibratory hub rolling moment between the uncoupled A and symmetric A optimum designs, normalized with steady torque; design condition is $\mu = 0.3$.

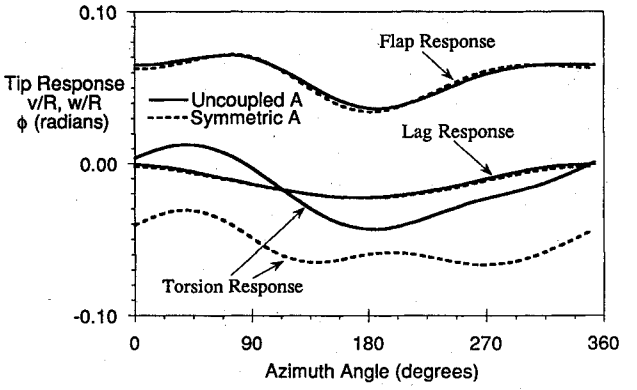

Fig. 7 Comparison of blade response between the uncoupled A and the symmetric A optimum designs, flap bending-torsion coupling.

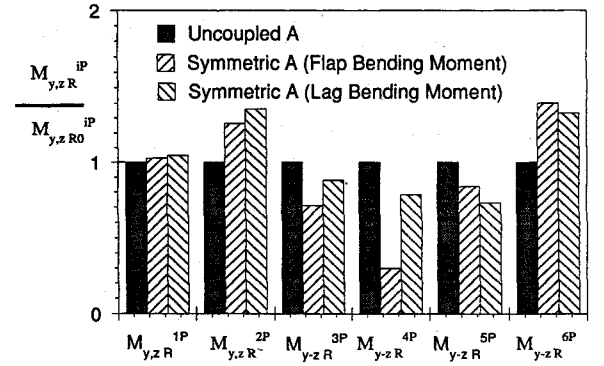

Fig. 8 Harmonics of vertical shear and flap bending moments at the blade root, normalized with uncoupled A values.

significant change in the magnitude and phase of the blade tip torsion response and very small change in the tip lag and flap response. When properly tailored, flap bending-torsion coupling acts as a vibration absorber for the blade, transferring energy between the flap and pitch motion and causing changes in the amplitude and phasing of the torsion response, resulting in reduction in the vibratory hub loads.

Minimizing the hub forces and moments in the fixed frame can result in an increase in the higher harmonic content of the vibratory forces and moments in the rotating frame since all harmonics are not covered by the objective function. Figure 8 show the first six harmonics of the blade root flap and lag bending moments corresponding to the uncoupled A optimum design and the symmetric A optimum design. It can be seen that whereas the 3, 4, and 5/rev harmonics of the bending moments are reduced, the 1, 2, and 6/rev harmonics are increased. Since the 3, 4, and 5/rev harmonics in the rotating frame are the source of the 4/rev harmonics in the fixed frame, their reduction decreases the objective function J; however,

this comes at the expense of increase in dynamic stresses caused by the increase in the 1, 2, and 6/rev harmonics in the rotating frame.

Optimization of Coupled Layups: Infeasible Starting Design

During the optimization iterations, the stability constraint is not violated, as can be seen from the damping values in Fig. 4. To make the stability constraint active during the design process, a margin of 3% damping is imposed on the blade lag mode. This results in all previous designs becoming infeasible. The optimization is then performed for the uncoupled A and the coupled layups. The optimizer selects the design variables to move the design into the feasible region. Only the symmetric D (negative lag bending-torsion coupling) achieves a feasible design. The uncoupled A, symmetric A, symmetric B, and symmetric C layups are unable to reach a feasible design point. For comparison, the uncoupled A design obtained earlier with zero margin on lag mode damping is used as the baseline design. The optimum design for the symmetric D case shows an increase in the lag mode damping of about 140% compared to the uncoupled A optimum design, as shown in Fig. 4. This improvement in lag mode damping; is brought about without much adverse effect on the flap and torsion mode dampings, however, there is an increase in the objective function of about 27% (Fig. 2). The optimum solution is $\theta_1 = 7, \theta_2 = 12, \theta_3 = 8$ deg.

This increase in lag mode damping is obtained at an advance ratio of 0.3. It is interesting to investigate if this optimum design also yields stability enhancement at other forward speeds. The lag damping for the uncoupled A design and the symmetric D optimum design are compared over a range of forward speeds in Fig. 9. Again, there is an enhancement in the lag mode stability over a range of forward speeds.

The blade flap, lag, and torsion response at the blade tip are shown for the uncoupled A optimum design and the symmetric D optimum in Fig. 10. There is a change in the phase of the torsion response, and the flap and lag response are almost unchanged. The increase in lag mode damping due to lag bending-coupling may be caused by a transfer of energy between the highly damped torsion mode and the low damped lag mode.

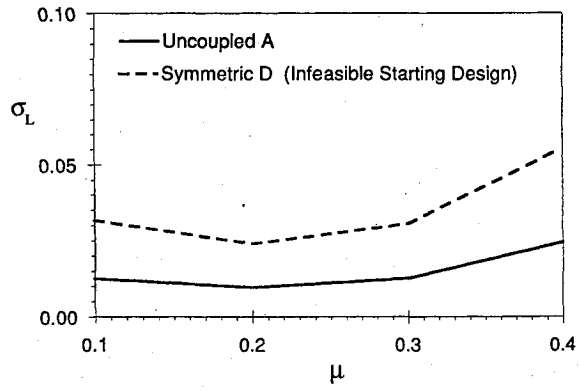

Fig. 9 Comparison of lag mode damping between the uncoupled A and the symmetric D optimum design.

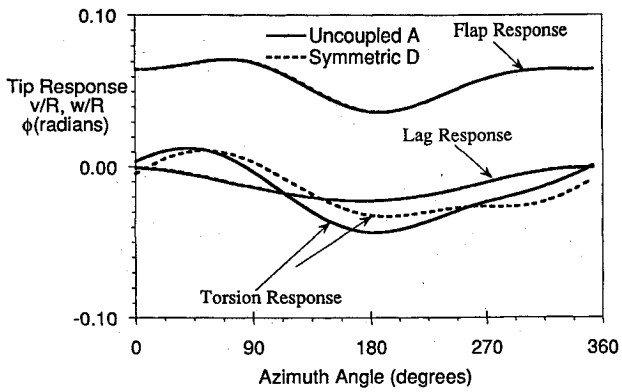

Fig. 10 Comparison of blade response between the uncoupled A and the symmetric D optimum, lag bending-torsion coupling, infeasible starting design.

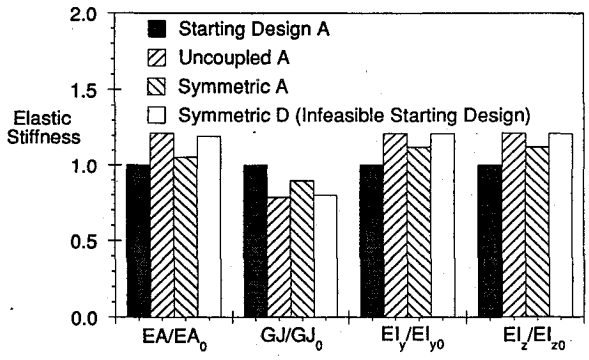

Fig. 11 Elastic stiffnesses for the uniform blade corresponding to initial and optimum designs, normalized with starting design A values.

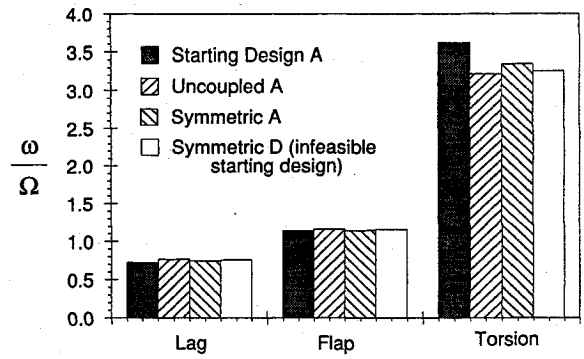

Fig. 12 Blade rotating frequencies of the first lag, flap, and torsion modes, corresponding to the initial and optimum designs.

Section Properties and Couplings

The section properties of the starting design A are compared with the uncoupled A, symmetric A, and symmetric D (infeasible starting design) optimum designs in Fig. 11. Relative to starting design A, the optimum designs are softer in torsion (GJ) and stiffer in flap (EI_y), lag (EI_z) and axial (EA) directions. These stiffnesses are uniformly distributed along the blade span.

The symmetric A design has positive flap bending-torsion coupling ($\bar{k}_{23} = 0.001024$) and the symmetric D design has negative lag bending-torsion coupling ($\bar{k}_{24} = 0.000841$), distributed uniformly along the blade span. To evaluate the conventional kinematic equivalents of the composite induced couplings, the uncoupled A, symmetric A, and symmetric D (infeasible) cases are examined in hover.

Using the conventional definition of flap bending-torsion coupling ($\Delta\theta = -K_p\beta$), we obtain $K_p = 0.6$ through composite coupling for the symmetric A layup. Normally, such flap bending-torsion coupling is introduced by skewing the flap hinge by an angle δ_3, which amounts to 31 deg for this case. As an example, the S-76 helicopter has a δ_3 angle of 17 deg. This shows that large amounts of flap bending-torsion coupling can be introduced by using composite tailoring.

Using the conventional definition of lag bending-torsion coupling ($\Delta\theta = -K_\zeta\zeta$) we have obtain K_ζ of -0.14 through composite coupling for the symmetric D (infeasible) layup. Normally, lag bending-torsion coupling is introduced by skewing the lag hinge by an angle δ_4, which amounts to -8 deg in this case. The negative lag bending-torsion coupling means that lag back produces nose-up pitch motion.

The rotating blade frequencies corresponding to these section properties are shown in Fig. 12. The flap and lag frequencies show small change from the starting design and the torsion frequency shows a reduction of as much as 10% from the starting design.

Refined Aerodynamic Modeling

All of the preceding results are based on quasisteady aerodynamic theory with a linear in-flow model. Although quasisteady aerodynamics appears acceptable at moderate flight conditions (at

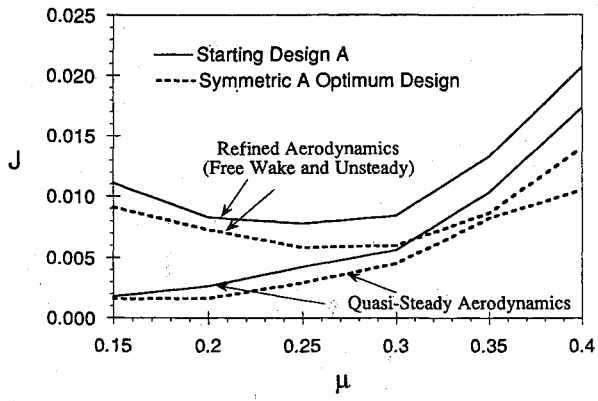

Fig. 13 Variation of objective function with forward speed for refined (free wake and unsteady) and quasisteady aerodynamic models, optimum solution is calculated at $\mu = 0.3$ with quasisteady aerodynamics.

which the aeroelastic optimization is performed), the unsteady effects become important at high forward speeds. The assumption of linear in-flow that is used in this investigation is expected to be satisfactory at moderate and high forward speeds where the wake is rapidly swept away from the rotor. However, at low forward speeds, the spatial and temporal gradients in circulation on the rotor disk leads to a complex wake structure that requires a free wake in-flow model. The unsteady aerodynamic model developed by Leishman and Beddoes[18] and the free wake model developed by Scully and Johnson[19] have been incorporated into the aeroelastic analysis UMARC.[13] Results obtained by performing the aeroelastic analysis with a free wake in-flow model and unsteady aerodynamics also show a reduction in the objective function at several forward speeds, even though the optimum design was obtained with a quasisteady aerodynamic model (Fig. 13).

Conclusions

Using an analytical formulation, rotor aeroelastic and sensitivity analyses are developed for a composite blade with a generic cross section. Shear effects are satisfactorily modeled using static condensation of the shear degrees of motion. For the numerical study, a four-bladed soft in-plane uniform hingeless rotor is investigated. The optimization problem consists of minimizing the 4/rev hub loads with constraints on frequency placement and aeroelastic stability in forward flight. The composite blade spar is modeled as a two-cell box beam. Design variables are the ply angles of the laminated walls of the composite box beams. The following conclusions are drawn from this study.

1) Compared to the starting design, a reduction of over 20% is obtained in the objective function due to the effects of elastic stiffnesses only. Positive flap bending-torsion coupling yields an additional reduction of 13% is obtained in the objective function.

2) Starting from an initially infeasible design with a stability margin of 3% in the lag mode, a coupled layup with negative lag bending-torsion coupling results in an increase in lag mode damping by about 140% compared to the optimum solution for the uncoupled blade. This increase in lag damping comes at the expense of an increase in the objective function of about 27%.

3) Even though the aeroelastic optimization is performed at a selected forward speed ($\mu = 0.3$), the optimum design for the symmetric A layup (positive flap bending-torsion coupling) shows a reduction in the 4/rev loads throughout the forward speed range. The beneficial effect of flap bending-torsion coupling for reduction of the vibratory loads increases at higher forward speeds. Also, for the symmetric D layup (negative lag bending-torsion coupling, infeasible design), there is an increase in blade lag mode damping for all forward speeds.

4) The benefits of composite coupling for reduction of vibratory loads and enhancement of blade stability come primarily from changes in the blade torsion response brought about by transfer of energy between the blade flap motion and pitch motion in flap bending-torsion coupled layups and between the blade lag motion and pitch motion in lag bending-torsion coupled layups.

5) The reductions in the 4/rev loads in the fixed frame can cause an increase in the magnitude of other harmonics in the rotating frame which are not covered by the objective function (like 1, 2, and 6/rev), resulting in an increase in blade dynamic stresses.

6) The aeroelastic optimization is performed using quasisteady aerodynamic modeling. With the inclusion of free wake and unsteady aerodynamic models, the optimum design shows comparable reductions in the vibratory hub loads in comparison to the quasisteady results.

Acknowledgments

This research is supported by the Army Research Office, Contract DAAH04-93-G-001. Technical Monitors are Robert Singleton and Tom Doligalski.

References

[1]Hong, C. H., and Chopra, I., "Aeroelastic Stability of a Composite Blade," *Journal of the American Helicopter Society*, Vol. 30, No. 2, 1985, pp. 29–35.

[2]Panda, B., and Chopra, I., "Dynamics of Composite Rotor Blades in Forward Flight," *Vertica*, Vol. 11, Nos. 1, 2, 1987, pp. 107–209.

[3]Smith, E. C., and Chopra, I., "Aeroelastic Response, Loads and Stability of a Composite Rotor in Forward Flight," *AIAA Journal*, Vol. 31, No. 7, 1993, pp. 1265–1274.

[4]Smith, E. C., and Chopra, I., "Air and Ground Resonance of Helicopters with Elastically Tailored Composite Rotor Blades," *Journal of the American Helicopter Society*, Vol. 38, No. 4, 1993, pp. 50–61.

[5]Friedmann, P. P., "Helicopter Vibration Optimization using Structural Optimization with Aeroelastic/Multidisciplinary Constraints," *Journal of Aircraft*, Vol. 28, No. 1, 1991, pp. 8–21.

[6]Davis, M. W., and Weller, W. H., "Helicopter Rotor Dynamics Optimization with Experimental Verification," *Journal of Aircraft*, Vol. 28, No. 1, 1991, pp. 38–48.

[7]Celi, R., and Friedmann, P. P., "Structural Optimization with Aeroelastic Constraints of Rotor Blades with Straight and Swept Tips," *AIAA Journal*, Vol. 28, No. 5, 1992, pp. 928–936.

[8]Vanderplatts, G. N., "Approximation Concepts for Numerical Airfoil Optimization," NASA TP-1370, March 1979.

[9]Lim, J., and Chopra, I., "Aeroelastic Optimization of a Helicopter Rotor using an Efficient Sensitivity Analysis," *Journal of Aircraft*, Vol. 28, No. 1, 1991, pp. 29–37.

[10]Kosmatka, J. B., and Friedmann, P. P., "Vibration Analysis of Composite Turbopropellers Using a Nonlinear Beam-Type Finite Element Approach," *AIAA Journal*, Vol. 27, No. 11, 1989, pp. 1606–1614.

[11]Smith, E. C., and Chopra, I., "Formulation and Evaluation of an Analytical Model for Composite Box Beams," *Journal of the American Helicopter Society*, Vol. 36, No. 3, 1991, pp. 23–35.

[12]Chandra, R., and Chopra, I., "Structural Behavior of Two-Cell Composite Rotor Blades with Elastic Couplings," *AIAA Journal*, Vol. 30, No. 12, 1992, pp. 2914–2924.

[13]Bir, G., et al., "University of Maryland Advanced Rotorcraft Code Theory Manual," Univ. of Maryland, UM-AERO Rept. 92-02, Jan. 1992.

[14]Nixon, M. W., and Hinnant, H. E., "Dynamic Analysis of Pretwisted Elastically-Coupled Rotor Blades," 1992 American Society of Mechanical Engineers Winter Annual Meeting, Anaheim, CA, Nov. 1992.

[15]Vanderplatts, G. N., "CONMIN—A Fortran Program for Constrained Function Minimization," User's Guide, NASA TMX 62282, Aug. 1973.

[16]Ganguli, R., and Chopra, I., "Aeroelastic Optimization of a Helicopter Rotor with Composite Tailoring," *Proceedings of the 49th Annual Forum and Technology Display of the American Helicopter Society*, St. Louis, MO, 1993, pp. 1335–1368.

[17]Watkins, R. I., and Morris, A. J., "A Multicriteria Objective Function Optimization Scheme for Laminated Composites for use in Multilevel Structural Optimization Schemes," *Computational Methods for Applied Mechanical Engineering*, No. 60, 1987, pp. 233–251.

[18]Leishman, J. G., and Beddoes, T. S., "A Generalized Model for Unsteady Aerodynamic Behavior and Dynamic Stall using the Indicial Method," *Journal of the American Helicopter Society*, Vol. 36, No. 1, 1990.

[19]Scully, M. P., "Computation of Helicopter Rotor Wake Geometry and its Influence on Rotor Harmonic Airloads," Massachusetts Inst. of Technology, MIT ASRL TR 178-1, Cambridge, MA, March 1975.